Available online at www.sciencedirect.com

ScienceDirect

Ceramics International 40 (2014) 4257–4266

CERAMICS INTERNATIONAL

www.elsevier.com/locate/ceramint

Investigation on low loss (1–x) $Mg_{0.95}Co_{0.05}TiO_3$–(x) $Ca_{0.6}La_{0.8/3}TiO_3$ composite series for achieving a nearly zero temperature coefficient of resonant frequency

Sunita Keshri*, Shailendra Singh Rajput

Department of Applied Physics, Birla Institute of Technology, Mesra, Ranchi 835215, India

Received 25 July 2013; received in revised form 20 August 2013; accepted 21 August 2013
Available online 30 August 2013

Abstract

This report presents the characteristic properties of $Mg_{0.95}Co_{0.05}TiO_3$(MCoT)−$Ca_{0.6}La_{0.8/3}TiO_3$(CLT) composite series, for achieving a material with large dielectric constant (ε_r), a high quality factor ($Q \times f$) and nearly zero temperature coefficient of resonant frequency (τ_f). By the help of Rietveld refinement method it is observed that the combination of MCoT (ilmenite-structured) and CLT (perovskite-structured) forms a two-phase system. The microwave dielectric properties have been measured using the Hakki–Coleman resonator method. The values of density, ε_r and τ_f have been theoretically obtained using existing models. A new material $0.80Mg_{0.95}Co_{0.05}TiO_3-0.20Ca_{0.6}La_{0.8/3}TiO_3$, possessing an excellent combination of dielectric properties with ε_r of 25.85, $Q \times f$ of 80,040 GHz (at 8.05 GHz) and $\tau_f \sim 0$ ppm/°C at 1300 °C, is investigated as a suitable material for microwave applications.

Keywords: Lichtenecker logarithmic model; Mixture rule; $MgTiO_3$–$CaTiO_3$; Temperature coefficient of resonant frequency

1. Introduction

The development of microwave communication systems requires materials which can be used as resonators in filters, antennas and oscillators at microwave frequencies in radar detectors, cellular telephones and global positioning satellite (GPS) devices [1,2]. In recent years several types of dielectric ceramic materials have been developed and investigated to match with the requirements of dielectric resonators [2]. For this the material must have three basic properties: high dielectric constant (ε_r), low dielectric loss or high quality factor ($Q \times f$) and near-zero temperature coefficient of resonant frequency (τ_f) at microwave frequencies [3]. This is because some of the key elements integrated within the dielectric in the high frequency circuits, such as filters and resonators need to be very stable against temperature fluctuation. For the development of dielectric ceramics with desirable properties, two conventional approaches are usually employed. One is to search a dielectric material, e.g. $Ba(Mg_{1/3}Ta_{2/3})O_3$ [4], $(Zr_{0.8}Sn_{0.2})TiO_4$[5] etc., in which the τ_f may be tuned by adjusting material's chemistry. The other method is to achieve composite by mixing two or more compounds with negative and positive τ_f values in order to compensate the τ_f value nearly zero [6,7].

The $MgTiO_3-CaTiO_3$ ceramic composite series is well known as the material for temperature stable dielectric resonators. The ceramic $0.95MgTiO_3-0.05CaTiO_3$ of this series gives $\varepsilon_r \sim 21$, $Q \times f \sim 56,000$ GHz (at 7 GHz) and $\tau_f \sim 0$ ppm/°C [8,9]. However, the required sintering temperature for this is too high (1450 °C) for practical applications. It is found that the dielectric properties of this composite series can be further improved by replacing Mg and Ca with suitable substitutions [8–12]. For example, the $0.85Mg_{0.95}Ni_{0.05}TiO_3-0.15Ca_{0.61}Nd_{0.26}TiO_3$ ceramic, sintered at 1350 °C, is found to possess $\varepsilon_r \sim 24.05$, $Q \times f \sim 67,000$ GHz and $\tau_f \sim -9.3$ ppm/°C [11]. Previously we have also found that the $0.79Mg_{0.95}Zn_{0.05}TiO_3-0.21Ca_{0.6}La_{0.8/3}TiO_3$ ceramic, sintered at 1275 °C shows good combination of dielectric properties with $\varepsilon_r \sim 26.26$, $Q \times f \sim 60,738$ GHz (at 6.44 GHz) and a nearly zero $\tau_f \sim -0.8$ ppm/°C [7].

*Corrresponding author. Tel.: +91 651 227 5444; fax: +91 651 227 5401.
E-mail addresses: sskeshri@rediffmail.com, s_keshri@bitmesra.ac.in (S. Keshri).

0272-8842/$ - see front matter © 2013 Elsevier Ltd and Techna Group S.r.l. All rights reserved.
http://dx.doi.org/10.1016/j.ceramint.2013.08.090

In this paper we report the structural, morphological and dielectric properties of the composite series $Mg_{0.95}Co_{0.05}TiO_3$ (MCoT)−$Ca_{0.6}La_{0.8/3}TiO_3$(CLT). We find that 0.80MCoT–0.20CLT sample, sintered at 1300 °C, shows nearly zero τ_f with higher $Q \times f$ as compared to that of our previous series. The XRD data of all samples have been analyzed using the Rietveld refinement method. The correlation between the microstructures and microwave dielectric properties has been investigated for this series. The experimental data of density, ε_r and τ_f have been compared with theoretical data, obtained using existing models.

2. Experimental

The composite samples (1–x)MCoT–(x)CLT with $x = 0.10$, 0.15, 0.20, 0.25 and 0.30 were synthesized by the conventional solid-state reaction method, as discussed in our previous report [7,12]. The corresponding samples will be hence after referred as 90MCoCLT, 85MCoCLT, 80MCoCLT, 75MCoCLT and 70MCoCLT respectively. The pellets were sintered at different temperatures in the range of 1200–1325 °C for 4 h in air. Phase purity and crystal structure of the samples at room temperature were identified using Bruker D8 Advance X-ray diffractometer, for the range $20^\circ \le 2\theta \le 80^\circ$ with a step size of 0.02. The X-rays were produced using a sealed tube and the wavelength of X-ray was 1.5406 Å (CuK_α). The X-rays were detected using a fast counting detector based on silicon strip technology (Bruker LynxEye detector). The structural analysis has been carried out by the well known Rietveld refinement method using FullProf software [13,14]. The Raman spectra were recorded at room temperature in a backscattering geometry, using a RENISHAW inVia Raman microscope attached with four standard Leica microscope objective lenses and an argon ion laser source with the excitation wavelength 514 nm. The spectra for the range of 100–1000 cm^{-1} were collected using 2400 lines/mm grating, with a 20 s data point acquisition time. The morphological and elemental analyses of the samples were obtained by JEOL scanning electron microscope (SEM); equipped with Oxford INCA Energy dispersive X-ray (EDX) Spectrometer.

The apparent density as well as apparent porosity of the grown samples was obtained using the Archimedes principle. In first step, the dry weight (D) of the sintered pellet was measured with a digital electronic balance. A glass beaker with the sample immersed in distilled water was kept in a vacuum chamber for 2 h. After that the beaker was taken out from the vacuum chamber. In this process the pores present in the pellet were completely filled with water. The weight of the pellet was again taken and interpreted as soaked weight (W). In second step, the sample was suspended in water with the help of a hanger to hang the pellet in water and the measured weight was interpreted as suspended weight (I). The apparent density ($\rho_{apparent}$) and apparent porosity were measured using the Archimedes principle

$$\rho_{apparent} = \frac{D}{W-I}, \tag{1}$$

$$\text{Apparent porosity} = \frac{W-D}{W-I} \tag{2}$$

The theoretical density (ρ_{theory}) has been calculated using the following formula [15]:

$$\rho_{theory} = \frac{ZA}{VN_A}, \tag{3}$$

where Z is number of atoms in unit cell, A is atomic weight (g/mol), V is volume of unit cell (cm^3) and N_A is Avogadro number (mol^{-1}). Relative density ($\rho_{relative}$) of sintered specimens has been calculated from the following equation:

$$\rho_{relative} = \frac{\rho_{apparent}}{\rho_{theory}} \tag{4}$$

Microwave dielectric properties of the composites were measured using TE_{011} resonance mode in a shielding cavity (designed by QWED, Poland) using Agilent PNA N5230A network analyzer with a weak or moderate coupling [16]. This method was first described by Hakki and Coleman [17]; according to them the dielectric constant can be calculated from the following equation:

$$\varepsilon_r = 1 + \left(\frac{c}{\pi D f_0}\right)(\alpha_1^2 + \beta_1^2), \tag{5}$$

where c is the velocity of light, α_1 can be obtained by the mode chart [18] and β_1 can be obtained from resonant frequency (f_0) and the sample dimension. This method was later analyzed and developed by Courtney [18], which was further improved by Kobayashi et al. [19,20]. In this paper, ε_r has been calculated using Eq. (5) and the loss tangent has been calculated using the formula of Kobayashi and Katho [20]:

$$\tan\,\delta = \frac{A}{l-1}\left(\frac{l}{Q_{ul}} - \frac{1}{Q_{u1}}\right), \tag{6}$$

where Q_{ul} is the unloaded quality factor of lth order and A is as described in Reference [20].

The temperature coefficient of resonant frequency (τ_f) of the sample was measured by introducing the cavity in a temperature controlled chamber [7]. The following equation was used for this calculation:

$$\tau_f = \frac{f_2 - f_1}{f_1(T_2 - T_1)}, \tag{7}$$

where f_1 and f_2 represent the resonant frequencies at two different temperatures T_1(~25 °C) and T_2 (~85 °C) respectively.

3. Results and discussions

3.1. XRD patterns

The room temperature XRD patterns of MCoT, CLT and (1−x)MCoT−(x)CLT samples sintered at 1300 °C for 4 h are shown in Fig. 1. The XRD patterns of composite samples illustrate the presence of ilmenite structured MCoT as the main crystalline phase and perovskite structured CLT as a minor phase suggesting the formation of a two-phase system. With the

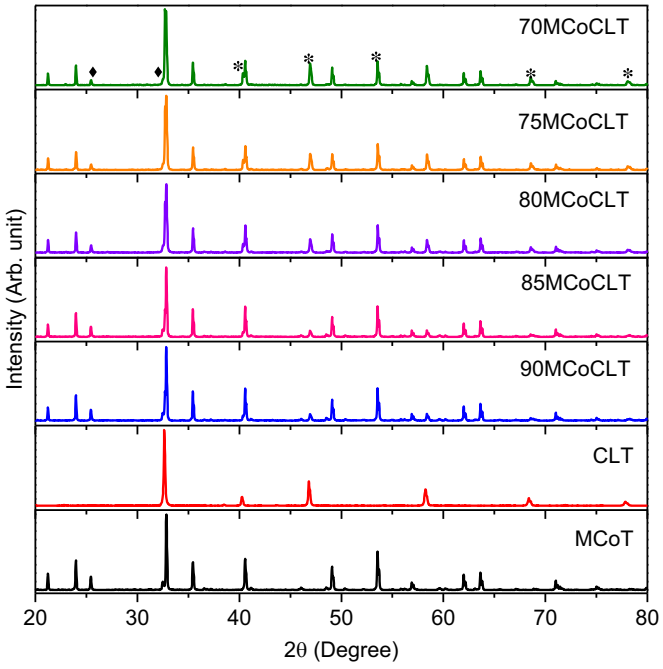

Fig. 1. XRD patterns of MCoT, CLT and (1–x)MCoT–(x)CLT samples, sintered at 1300 °C [◆: $Mg_{0.95}Co_{0.05}Ti_2O_5$, ✻: CLT].

increase of x, CLT phase is gradually enhanced, the peaks due to CLT are marked with '✻'. The XRD pattern of MCoT phase is in good agreement with hexagonal structure according to the Joint Committee on Powder Diffraction Standards (JCPDS) card no. 06-0494, whereas CLT phase shows good agreement with orthorhombic structure of $CaTiO_3$ corresponding to JCPDS card no. 22-0153. In the XRD patterns the peaks indicated by '◆' arise because of the $Mg_{0.95}Co_{0.05}Ti_2O_5$ phase. This is usually formed as an intermediate phase and is difficult to completely eliminate from the sample prepared by the mixed oxide route.

The XRD data of all samples have been analyzed using the Rietveld refinement method and refined results are shown in Fig. 2(a)–(c). From the XRD results it is confirmed that the MCoT sample has two phases: main phase MCoT and impurity phase $Mg_{0.95}Co_{0.05}Ti_2O_5$ (Fig. 1). Hence XRD data of this sample have been refined using a mixture model of two phases. The refinement has been carried out initially taking the positional parameters of hexagonal structure of MCoT [7] and orthorhombic structure of $Mg_{0.95}Co_{0.05}Ti_2O_5$ [21]. The occupancy factors for the mixed Mg and Co sites for both phases have been fixed at the nominal composition. Successful refinement confirms that the main phase of this sample has hexagonal structure with $R\bar{3}$ space group and the lattice parameters: $a=b=5.0674$ Å and $c=13.9291$ Å. Its impurity phase has orthorhombic structure with *Bbmm* space group and lattice parameters: $a=9.7587$ Å, $b=10.0081$ Å and $c=3.7483$ Å. The weight (mass) fractions of hexagonal and orthorhombic phases based on the refined scale factors are found to be 96.91% and 3.09% respectively. The refinement results of CLT ceramic are shown in Fig. 2(b). The refinement is done, initially by taking positional parameters of orthorhombic structure with *Pbnm* space group of $CaTiO_3$ [22]. The occupancy factors for the mixed Ca and La sites have been fixed at the nominal composition. Successful refinement confirms that CLT ceramic has orthorhombic structure with *Pbnm* space group and the lattice parameters are: $a=5.4804$ Å, $b=5.4929$ Å and $c=7.7512$ Å. It is noteworthy to point out that the CLT phase generally shows either of pseudo-cubic [23] or orthorhombic [24,25] structures. In our recent article [7] we have reported that XRD data of CLT can be fitted well to cubic structure with $Pm\bar{3}m$ space group. But more thorough investigation of such fittings has led us understand that the XRD data of CLT can be fitted more preciously with orthorhombic structure as mentioned above.

For the refinement of 80MCoCLT composite sample a mixture model of three phases (MCoT, $Mg_{0.95}Co_{0.05}Ti_2O_5$ and CLT) has been used and obtained results are shown in Fig. 2(c). The refinement results reveal that 80MCoCLT ceramic is mixture of hexagonal structured MCoT with $R\bar{3}$ space group, orthorhombic structured $Mg_{0.95}Co_{0.05}Ti_2O_5$ with *Bbmm* space group and orthorhombic structured CLT with *Pbnm* space group. The weight fraction of MCoT, $Mg_{0.95}Co_{0.05}Ti_2O_5$ and CLT phases based on the refined scale factors are found to be 79.34%, 2.55% and 18.11% respectively. On the basis of refined crystallographic data, it can be concluded that a good agreement is achieved between the calculated and observed XRD patterns. The Wyckoff positions and crystallographic data of 80MCoCLT composite, sintered at 1300 °C, after refinement using the Fullprof program are demonstrated in Table 1. The obtained lattice parameters and goodness of fit indicator (χ^2) for all composite samples, sintered at 1300 °C, are listed in Table 2. This study clearly indicates the coexistence of both the phases in composite samples without any detectable amount of interdiffusion between them. The Rietveld method has also been successfully applied for determination of the quantitative phase analysis (QPA) of the composite materials [26]. There is a simple relationship between the individual scale factor determined, considering all refined structural parameters of individual phases of a multiphase sample and the phase concentration (volume/weight fraction) in the mixture. The QPA resulted from the refinement procedure is summarized in Table 3. One can observe that the QPA is in good agreement with the composition of each composite phase in the samples investigated.

The XRD patterns of 80MCoCLT sample, sintered at various temperatures in the range 1200–1325 °C, are shown in Fig. 2(d). It is evident from the figure that the patterns remain almost unaltered with sintering temperature. However, the peak corresponding to the $Mg_{0.95}Co_{0.05}Ti_2O_5$ phase has become more prominent for the samples sintered at higher temperatures.

3.2. Raman spectra

The Raman spectra of MCoT, CLT and 80MCoCLT samples are shown in Fig. 3(a)–(c). According to the description in the Bilbao crystallographic center website [27], the ilmenite structure $MgTiO_3$ has ten Raman-active vibrational modes($\Gamma_{Raman}=5A_g+5E_g$), which supports our findings. The A_g (225.7 and 306.1 cm^{-1}) modes occur because of the vibrations of Mg and Ti atoms along the z-axis. The others A_g modes observed at 397.7, 498.8 and 714.7 cm^{-1} are attributed to the vibrations of O atoms.

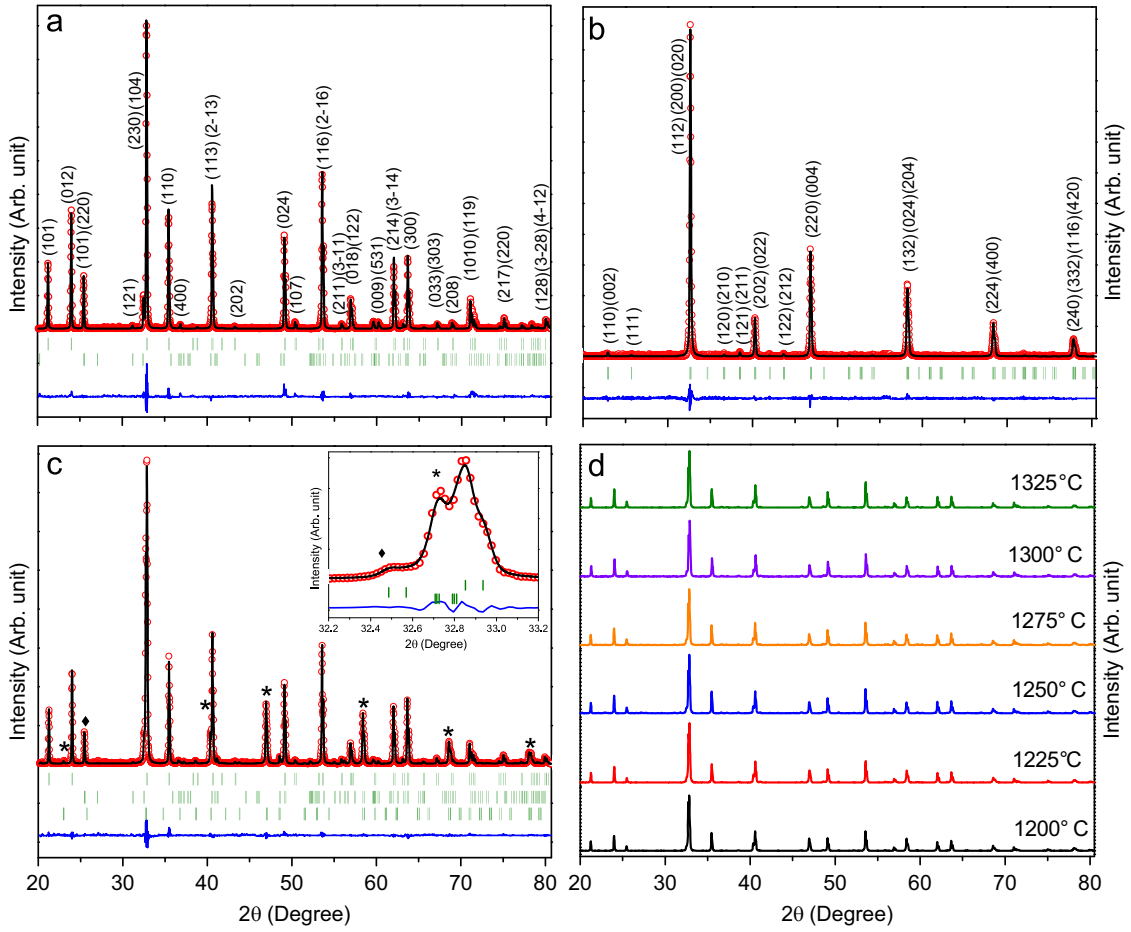

Fig. 2. Observed (open symbols) and calculated (solid lines) XRD patterns for (a) MCoT, (b) CLT and (c) 80MCoCLT. Differences between the observed and the calculated intensities are shown at the bottom of the figure. The calculated Bragg–reflected positions are marked by the vertical bars. The Miller indices of the major Bragg reflections are also indicated. (d) XRD patterns of 80MCoCLT ceramic, sintered at different sintering temperatures.

Table 1
Rietveld refinement results and atomic coordinates employed in order to model the MCoT and CLT unit cells.

Sample	Symmetry and space group	Atoms	Site	Atomic coordinate		
				x	*y*	*z*
MCoT		Mg/Co	6c	0.0	0.0	0.3584
	Hexagonal	Ti	6c	0.0	0.0	0.1453
	S.G.–$R\bar{3}$	O1	18f	0.3171	0.0159	0.2360
CLT		Ca/La	4c	0.0121	0.0146	0.25
	Orthorhombic	Ti	4b	0.0	0.5	0.0
	S.G. – *Pbnm*	O1	4c	−0.0101	0.5132	0.25
		O2	8d	0.7506	0.2872	0.0198

$R_p = 10.7$, $R_{wp} = 16.3$, $R_{exp} = 13.0$, $R_{Bragg} = 4.16$ (MCoT) and $R_{Bragg} = 6.56$ (CLT)

For A_g modes (498.8 and 714.7 cm^{-1}), the six O atoms of octahedral configuration present breathing-like vibrations, but each with different vibration directions. The intense E_g mode appeared at 281.8 cm^{-1} is related to the anti-symmetric breathing vibration of the O octahedron. The E_g modes (327.9 and 352 cm^{-1}) can be described as the twisting of the O octahedron with the vibrations of Mg and Ti atoms parallel to the *xy*–plane. The E_g (484.7 cm^{-1}) mode arises due to the anti-symmetric breathing vibration of the O octahedra with the cationic vibrations of both Mg and Ti atoms parallel to the *xy*–plane, while the E_g (640.7cm^{-1}) mode is related to the anti-symmetric twisting vibration of the O octahedra associated with the Ti–O stretching [28,29]. The perovskite structured CLT shows 8 Raman modes as shown in Fig. 3(b). According to the literature [30,31], orthorhombic

structure with space group *Pbnm*, has 24 Raman-active modes, which can be described by the representation $\Gamma_{\text{Raman,Pbnm}} = 7A_g + 7B_{1g} + 5B_{2g} + 5B_{3g}$. The Raman band B_{2g} (116.1 cm^{-1}) is related to the Ca−TiO_3 lattice mode. The bands A_g (163.4 and 285.3 cm^{-1}), B_{1g} (219.5 cm^{-1}) and B_{3g} (330.8 cm^{-1}) are assigned to O–Ti–O bending modes. The band A_g (461.2 cm^{-1}) is related to Ti−O_6 torsional modes. The other bands at 399.6 and 513.8 cm^{-1} might be related to Raman bands of $LaTiO_3$. The peak at 796.5 cm^{-1} is related to B_{2g} mode. In Raman spectrum of CLT, fewer bands are observed possibly due to very low polarizability, so as to prevent such bands from being seen in the spectrum. Fig. 3(c) shows the Raman spectra of (1−*x*)MCoT−(*x*)CLT composite samples. Most of the active Raman modes of these spectra correspond to MCoT phase, but with a small shift at lower wave number as illustrated in the inset. Only some of the peaks of CLT phase remain clear (marked with "#"); this may be because of the fact that most of the peak positions of this phase are closer to those of MCoT phase. It is observed that the peak intensity of composite samples decreases with CLT addition.

3.3. Microstructural and elemental analysis

Fig. 4 shows the surface microstructural images of the 80MCoCLT composite sintered at different temperatures in the range 1200–1325 °C. The image of Fig. 4(a) indicates that the specimen does not appear dense and the grains of small size are grown at 1200 °C. The grain size increases as the sintering temperature increases. The pores are almost eliminated for the sample sintered at 1300 °C and a noticeable grain growth and a relatively uniform surface morphology are observed at this temperature. However, inhomogeneous grain growth is monitored at temperature 1325 °C with melted and porous microstructures, which might degrade the microwave dielectric properties of the ceramics. In order to analyze the composition, the EDX results of 80MCoCLT composite sample are demonstrated in Fig. 4(g) and (h) for two different positions of Fig. 4 (e). Spots 'A' and 'B' show mostly the expected peaks of MCoT and CLT phases respectively; the Pt peaks in the EDX spectra come from the coating of platinum over the surface of sample required to avoid charging.

Table 2
The goodness of fit indicator (χ^2) and lattice parameter of (1–*x*)MCoT–(*x*)CLT composite samples, sintered at 1300 °C.

Samples	MCoT		CLT			χ^2
	a (Å)	*c* (Å)	*a* (Å)	*b* (Å)	*c* (Å)	
90MCoCLT	5.0619	13.9217	5.4716	5.4721	7.7272	1.92
85MCoCLT	5.0665	13.9223	5.4691	5.4743	7.2775	2.61
80MCoCLT	5.0654	13.9214	5.4713	5.4692	7.7269	1.96
75MCoCLT	5.0683	13.9232	5.4734	5.4698	7.7267	2.25
70MCoCLT	5.0642	13.9191	5.4695	5.4734	7.7283	2.18

3.4. Densification studies

The apparent density of the (1–*x*)MCoT–(*x*)CLT composite samples with different *x* values is shown in Fig. 5(a) as a function of sintering temperature. Initially there is a significant increase in density with increasing sintering temperature, it becomes maximum at 1300 °C and thereafter trend of variation is reversed. The degradation of density at temperature above 1300 °C occurs due to the inhomogeneous grain growth and partial melting of grain boundaries, as understood from SEM studies [See Fig. 4(f)]. It can also be observed that density of the sample enhances with increasing CLT content, since the density of CLT is relatively higher (~4.73 g/cm^3) than that of MCoT (~3.59g/cm^3). At 1300 °C, the apparent density of the composite samples lies in the range 3.78–4.05 g/cm^3 respectively. For a two-phase composite sample, the theoretical density of the composite can be calculated using mixing model [26] as given below

$$\frac{1}{\rho_{\text{composite}}} = \frac{(1-x)}{\rho_1} + \frac{x}{\rho_2}, \tag{8}$$

where *x* is weight% (wt%) of second phase, ρ_1 and ρ_2 are the theoretical density of first and second phases respectively; these values have been obtained from the Rietveld refinement. The values of apparent density, theoretical density, relative density and apparent porosity of all composite samples, sintered at 1300 °C are listed in Table 3. It is evident from this table that the apparent density determined experimentally is slightly less than theoretical density, because the macroscopic specimen usually contains minute cracks and pores.

Table 3
The values of apparent density, apparent porosity, theoretical density and relative density of composite samples, sintered at 1300 °C.

Sample	Weight fraction (%)		Density			Apparent porosity
	MCoT*	CLT	Theoretical ρ (g/cm^3)	Experimental ρ (g/cm^3)	Relative ρ (%)	
90MCoCLT	90.07	9.93	4.038	3.776	93.503	1.403E-5
85MCoCLT	84.69	15.31	4.101	3.895	94.989	1.089E-5
80MCoCLT	81.89	18.11	4.129	3.959	95.880	3.693E-6
75MCoCLT	74.68	25.32	4.210	3.986	94.680	4.062E-5
70MCoCLT	70.86	29.14	4.252	4.046	95.152	3.737E-6

*Weight fraction of $Mg_{0.95}Co_{0.05}Ti_2O_5$ is included.

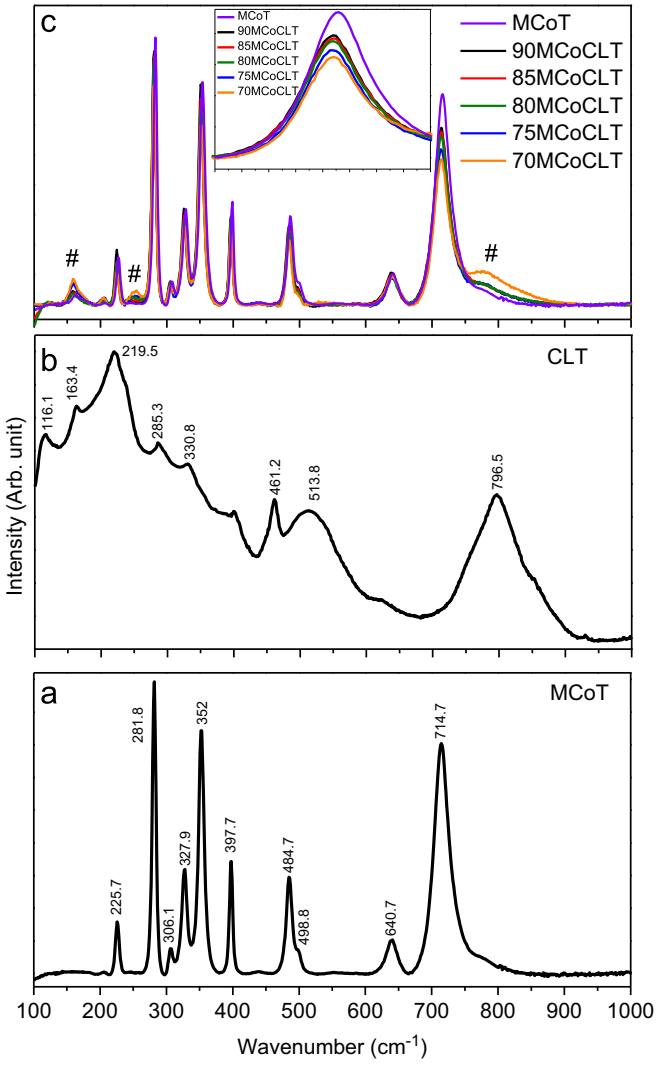

Fig. 3. Raman spectra of (a) MCoT, (b) CLT and (c) (1–*x*)MCoT–(*x*)CLT samples. The mode appeared at 715 cm^{-1} has been enlarged in the inset.

3.5. Microwave dielectric properties

The dielectric constant (ε_r) of the composites as a function of sintering temperature, is depicted in Fig. 5(b). The dependence of ε_r as a function of sintering temperature shows the same trend as obtained between density and sintering temperature. The value of ε_r increases with increasing sintering temperature. After reaching its maximum at 1300 °C, it decreases. It is also observed that the value of ε_r for composite samples increases as the x value increases, because of the fact that CLT has a much higher ε_r (~113.35) compared to that (~16.54) of MCoT. For MCoCLT series, sintered at 1300 °C, the ε_r values have been found to lie in the range 21.67–31.52.

The theoretical ε_r of two-phase MCoT–CLT composites, sintered at 1300 °C, has been calculated using different mixing formulae based on the effective medium models [32–36]. The mathematical equations of each model are described as follows:

Series mixing model [32]

$$\frac{1}{\varepsilon_r} = \frac{(1-x)}{\varepsilon_{r_1}} + \frac{x}{\varepsilon_{r_2}}, \tag{9}$$

Parallel mixing model [33]

$$\varepsilon_r = (1-x)\,\varepsilon_{r_1} + x\varepsilon_{r_2}, \tag{10}$$

Brick–wall model [34]

$$\varepsilon_r = \varepsilon_{r_2}\left(1-\frac{1-x}{1-n}\right) + \left(\frac{1-x}{1-n}\right)\frac{\varepsilon_{r_1}\varepsilon_{r_2}}{(1-n)\varepsilon_{r_2} + n\,\varepsilon_{r_1}}, n = 1/3x; \tag{11}$$

Lichtenecker empirical logarithmic model [35]

$$\ln \varepsilon_r = (1-x)\ln \varepsilon_{r_1} + x \ln \varepsilon_{r_2}; \tag{12}$$

Calusius–Mossotti equation [36]

$$\frac{\varepsilon_r - 1}{\varepsilon_r + 2} = (1-x)\frac{\varepsilon_{r_1} - 1}{\varepsilon_{r_1} + 2} + x\frac{\varepsilon_{r_2} - 1}{\varepsilon_{r_2} + 2}, \tag{13}$$

where x is the wt% of CLT phase, ε_{r_1} and ε_{r_2} are the relative permittivities of MCoT and CLT phases respectively. The experimental values of ε_r and its theoretical values, calculated using different models are plotted in Fig. 6 with the variation of the CLT content. From the figures it is observed that in the considered range, the data calculated using series mixing model

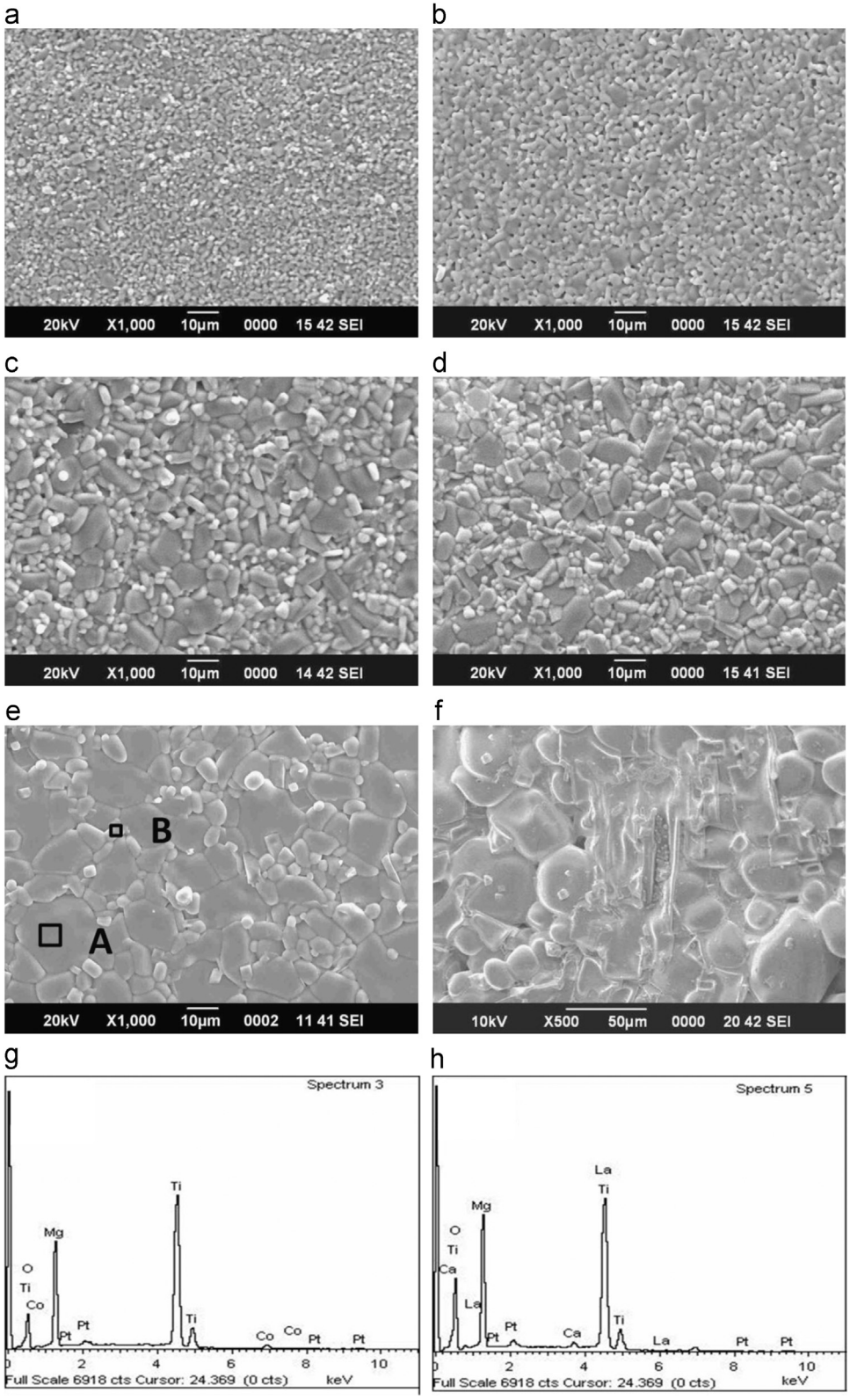

Fig. 4. SEM micrographs of 80MCoCLT sample, sintered at (a) 1200 °C, (b) 1225 °C, (c) 1250 °C, (d) 1275 °C, (e) 1300 °C and (f) 1325 °C; (g) and (h) EDX results for positions 'A' and 'B' respectively.

as well as Calusius–Mossotti equation are quite small as compared to the experimental data. On the other hand, the parallel mixing model gives overestimated values of ε_r. We have observed that there are two appropriate models in this case. The first is the Lichtenecker empirical logarithmic rule, which is often used for the mixtures of powders or porous systems. The second appropriate formula is the Brick–Wall model, which explains the exact solution for the dielectric constant of a mixture of coated

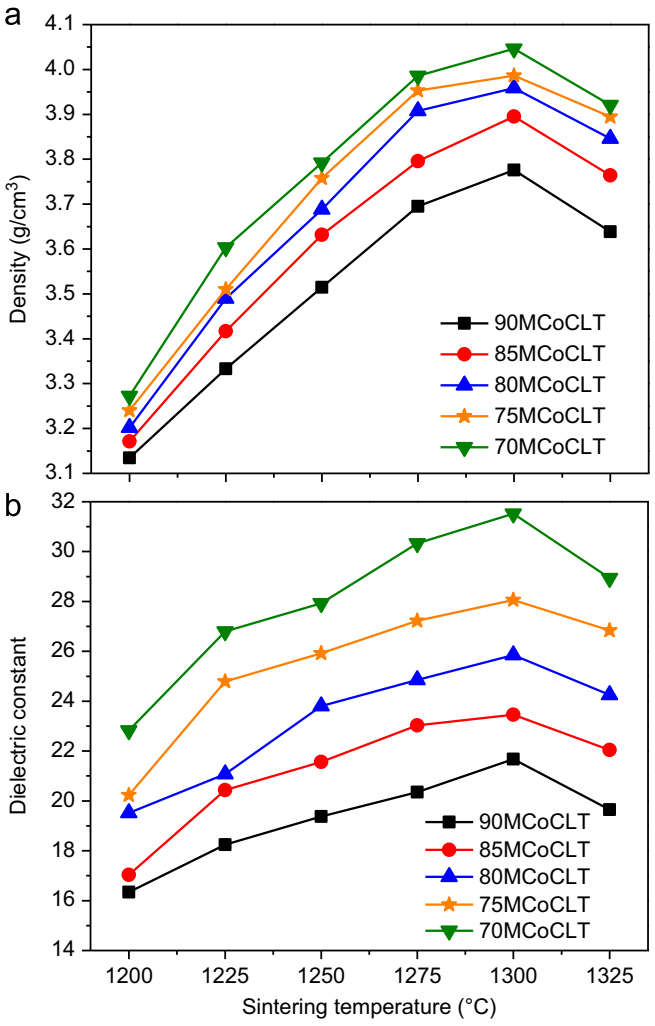

Fig. 5. Apparent density and dielectric constant of composite samples as a function of sintering temperature.

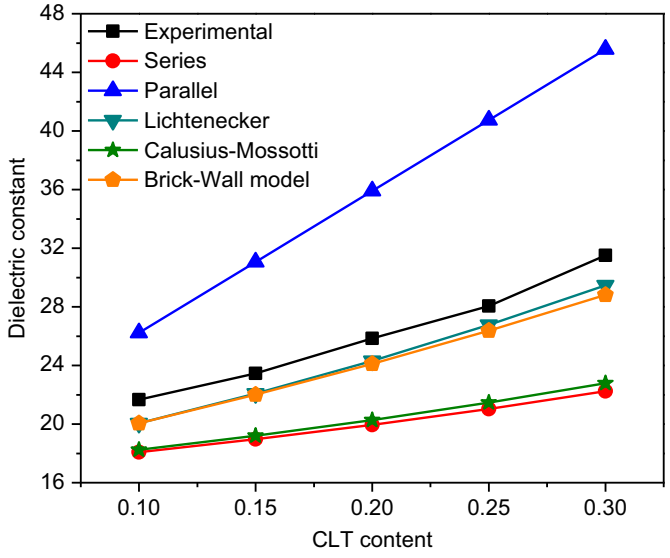

Fig. 6. The experimental and theoretical dielectric constant of (1–x)MCoT–(x)CLT composites, sintered at 1300 °C, as a function of CLT content.

spheres. However, the small deviation in ε_r corresponding to these two models may be because of the dissimilar microstructural shapes of both the phases [37]. This might have occurred also because of the presence of porosity and the impurity phase $Mg_{0.95}Co_{0.05}Ti_2O_5$ having a relative permittivity ~17.56 [38].

Fig. 7(a) presents the $Q \times f$ values of different samples of this series as a function of sintering temperature. From this figure it is observed that the $Q \times f$ of composites decreases with increasing CLT content because the $Q \times f$ of CLT is (~16,730 GHz at 2.93 GHz) lower than that of MCoT (~198,370 GHz at 8.03 GHz). It is also examined that with increasing sintering temperature, the $Q \times f$ value increases to a maximum and thereafter it decreases. The maximum $Q \times f$ value of each composition of this series arises corresponding to the sintering temperature 1300 °C. With sintering temperature the enhancement in $Q \times f$ of a composition can be attributed to the increase in density and grain size, decrease in pores and the grain boundary area as well as the uniformity of grain growth. A degradation of $Q \times f$ value for the sample, sintered at 1325 °C, has been noticed because of its lesser density resulted from the inhomogeneous grain growth and melted microstructures [Fig. 4(f)]. The formation of impurity

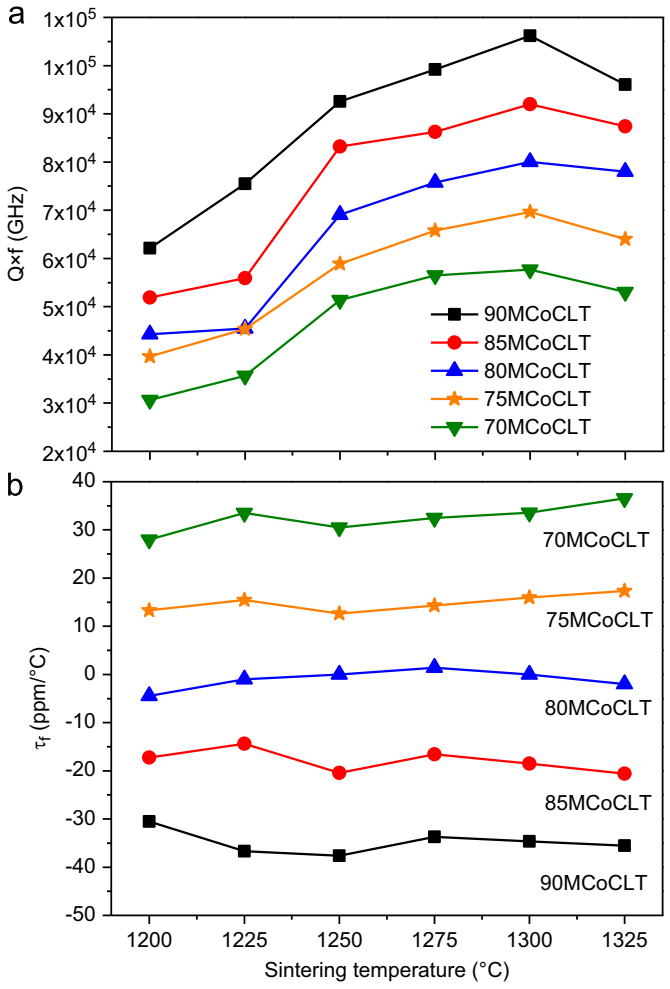

Fig. 7. (a) $Q \times f$ and (b) τ_f values of composite samples with the variation of sintering temperature.

Table 4
The microwave dielectric properties of (1–x)MCoT–(x)CLT composite samples, sintered at 1300 °C.

Sample	ε_r	$Q \times f$ (GHz)	τ_f (ppm/°C)	
			Measured	Calculated
90MCoCLT	21.67	106,180	−34.6	−26.6
85MCoCLT	23.46	91,980	−18.5	−12.4
80MCoCLT	25.85	80,040	0.002	1.8
75MCoCLT	28.06	69,660	16.0	16.0
70MCoCLT	31.52	57,680	33.6	30.2

phase $Mg_{0.95}Co_{0.05}Ti_2O_5$, as confirmed by XRD studies (Fig. 1) may also cause a decrease in the $Q \times f$ value because it has lower quality factor (~58,000 GHz) [38].

The τ_f values of (1–x)MCoT–(x)CLT composites, sintered at different temperatures are demonstrated in Fig. 7(b). From this figure it is evident that τ_f is insensitive to the sintering temperature for the entire temperature range under consideration. However, the τ_f value has been found to be related to the weight percentage of the second phase. Since the τ_f values of MCoT and CLT are –55 and 229 ppm/°C respectively, the τ_f values of these composites rapidly become more positive with increasing CLT content. Its value becomes ~0 for 80MCo CLT sample. The τ_f of the mixture phases has been computed using a general mixture rule [37] as given below

$$\tau_f = (1-x)\tau_{f_1} + (x)\tau_{f_2}, \quad (14)$$

where x is wt% of the CLT phase, τ_{f_1} and τ_{f_2} are temperature coefficients of MCoT and CLT phases respectively. The obtained data have been compared with experimental results as illustrated in Table 4. It is evident that the experimental results of τ_f slightly deviate from the corresponding calculated results obtained using mixture rule.

Form Figs. 5(b), 7(a) and (b), we can notice that out of all composite samples the $0.80Mg_{0.95}Co_{0.05}TiO_3$–$0.20Ca_{0.6}La_{0.8/3}TiO_3$ ceramic sintered at 1300 °C shows best combination of microwave dielectric properties (ε_r ~25.85, $Q \times f$ ~80,040 GHz at 8.05 GHz and τ_f ~0 ppm/°C). Its quality factor is higher compared to the similar sample (sintered at 1275 °C) with nearly zero τ_f of our previous series $Mg_{0.95}Zn_{0.05}TiO_3 - Ca_{0.6}La_{0.8/3}TiO_3$, whereas ε_r is almost same for both samples.

4. Conclusions

Characteristic properties of (1−x)MCoT–(x)CLT composite ceramics have been studied in order to achieve a thermal stable material with good combination of dielectric properties. All composite samples exhibit mixed phases of MCoT (ilmenite-structured) as the main phase in association with second phase CLT (perovskite-structured) and an impurity phase $Mg_{0.95}Co_{0.05}Ti_2O_5$. The detailed structural study has been done by employing the Rietveld refinement technique with the help of the FullProf suite program. The microwave dielectric properties are strongly related to the density, percentage of second phase, sintering temperature and microstructure of the sample. It is found that with the increase in CLT content, the ε_r of the composite samples increases whereas its quality factor decreases. The values of density, ε_r and τ_f have been theoretically obtained using existing models. Deviation between theoretical and experimental results might have occurred due to the dissimilar microstructural shapes of both the phases. It is concluded that the values of ε_r of these samples can be explained well using the Lichtenecker empirical logarithmic rule as well as the Brick–wall model. The composite with $x = 0.20$ can be considered as a suitable material for DRs.

Acknowledgments

The author, S. Keshri gratefully acknowledges Department of Science and Technology, India for funding the project. The other author, S.S. Rajput gratefully acknowledges Council of Scientific and Industrial Research, India for financial assistance. Both the authors are thankful to the members of Central Instrumentation Facility Lab, Birla Institute of Technology Ranchi, India for providing SEM and EDX facilities. The authors acknowledge the support of Mr. Rajkishor Pramanik in fabrication and associated experimentation. The X-ray analysis was performed at UGC-DAE Consortium for Scientific Research, Indore; Dr. Mukul Gupta is acknowledged for supporting this work. The authors are thankful to Dr. Nisha Gupta and Dr. Vibha Rani Gupta, Department of ECE, Birla Institute of Technology, Ranchi, India for extending support of dielectric measurements.

References

[1] H. Ohsato, Functional advances of microwave dielectrics for next generation, Ceramics International 38 (2012) S141–S146.
[2] I.M. Reaney, D. Iddles, Microwave dielectric ceramics for resonators and filters in mobile phone networks, Journal of the American Ceramic Society 89 (2006) 2063–2072.
[3] S.B. Narang, S. Bahel, Low loss dielectric ceramics for microwave applications: a review, Journal of Ceramic Processing Research 11 (2010) 316–321.
[4] T. Shimada, K. Ichikawa, T. Minemura, T. Kolodiazhnyi, J. Breeze, N. M. Alford, G. Annino, Temperature and frequency dependence of dielectric loss of $Ba(Mg_{1/3}Ta_{2/3})O_3$ microwave ceramics, Journal of the European Ceramic Society 30 (2010) 331–334.
[5] D. Pamu, G.L.N. Rao, K.C.J. Raju, Enhanced microwave dielectric properties of $(Zr_{0.8}Sn_{0.2})TiO_4$ ceramics with the addition of its own nanoparticles, Journal of the American Ceramic Society 95 (2012) 126–132.
[6] D. Zhou, L.X. Pang, J. Guo, Z.M. Qi, T. Shao, X. Yao, C.A. Randall, Phase evolution, phase transition, and microwave dielectric properties of scheelite structured $xBi(Fe_{1/3}Mo_{2/3})O_4 - (1-x)BiVO_4 (0.0 \le x \le 1.0)$ low temperature firing ceramics, Journal of Materials Chemistry 22 (2012) 21412–21419.
[7] S.S. Rajput, S. Keshri, V.R. Gupta, Microwave dielectric properties of $(1-x)Mg_{0.95}Zn_{0.05}TiO_3 - (x)Ca_{0.6}La_{0.8/3}TiO_3$ ceramic composites, Journal of Alloys and Compounds 552 (2013) 219–226.
[8] K. Wakino, Recent development of dielectric resonator materials and filters in Japan, Ferroelectrics 91 (1989) 69–86.
[9] Y.C. Chen, S.M. Tsao, C.S. Lin, S.C. Wang, Y.H. Chien, Microwave dielectric properties of $0.95MgTiO_3 - 0.05CaTiO_3$ for application in dielectric resonator antenna, Journal of Alloys and Compounds 471 (2009) 347–351.
[10] V.M. Ferreira, F. Azough, R. Freer, J.L. Baptista, The effect of Cr and La on $MgTiO_3$ and $MgTiO_3 - CaTiO_3$ microwave dielectric ceramics, Journal of Materials Research 12 (1997) 3293–3299.

[11] C.H. Shen, C.L. Huang, C.F. Shih, C.M. Huang, The effect of $Ca_{0.61}Nd_{0.26}$-TiO_3addition on the microwave dielectric properties of $(Mg_{0.95}Ni_{0.05})TiO_3$ ceramics, Journal of Alloys and Compounds 475 (2009) 391–395.
[12] S.S. Rajput, S. Keshri, V.R. Gupta, N. Gupta, V. Bovtun, J. Petzelt, Design of microwave dielectric resonator antenna using MZTO-CSTO composite, Ceramics International 38 (2012) 2355–2362.
[13] R.A. Young, The Rietveld Method, Oxford University Press, New York, 1993.
[14] H.M. Rietveld, A profile refinement method for nuclear and magnetic structures, Journal of Applied Crystallography 2 (1969) 65–71.
[15] B.D. Cullity, Elements of X-ray Diffraction, 2nd Ed., Addison-Wesley Publishing Company, Inc., 1978.
[16] J. Krupka, Frequency domain complex permittivity measurements at microwave frequencies, Measurement Science and Technology 17 (2006) R55–R70.
[17] B.W. Hakki, P.D. Coleman, A dielectric resonator method of measuring inductive capacities in the millimeter range, IRE Transactions on Microwave Theory and Techniques 8 (1960) 402–410.
[18] W.E. Courtney, Analysis and evaluation of a method of measuring the complex permittivity and permeability of microwave insulators, IEEE Transactions on Microwave Theory and Techniques 18 (1970) 476–485.
[19] Y. Kobayashi, S. Tanaka, Resonant modes of a dielectric rod resonator short-circuited at both ends by parallel conducting plates, IEEE Transactions on Microwave Theory and Techniques 28 (1980) 1077–1086.
[20] Y. Kobayashi, M. Katoh, Microwave measurement of dielectric properties of low-loss materials by the dielectric rod resonator method, IEEE Transactions on Microwave Theory and Techniques 33 (1985) 586–592.
[21] H. Yang, R.M. Hazen, Crystal chemistry of cation order–disorder in pseudobrookite-Type $MgTi_2O_5$, Journal of Solid State Chemistry 138 (1998) 238–244.
[22] L.S. Cavalcante, V.S. Marques, J.C. Sczancoski, M.T. Escote, M.R. Joya, J. A. Varela, M.R.M.C. Santos, P.S. Pizani, E. Longo, Synthesis, structural refinement and optical behavior of $CaTiO_3$ powders: A comparative study of processing in different furnaces, Chemical Engineering Journal 143 (2008) 299–307.
[23] I.S. Kim, W.H. Jung, Y. Inaguma, T. Nakamura, M. Itoh, Dielectric properties of A-site deficient perovskite-type lanthanum–calcium–titanium oxide solid solution system $[(1-x)La_{2/3}TiO_3-xCaTi03 \quad (0.1 \le x \le 0.96)]$, Materials Research Bulletin 30 (1995) 307–316.
[24] Y. Li, S. Qin, F. Seifert, Phase transitions in A-site substituted perovskite compounds: The $(Ca_{1-2x}Na_xLa_x)TiO_3 (0 \le x \le 0.5)$ solid solution, Journal of Solid State Chemistry 180 (2007) 824–833.
[25] C.L. Huang, J.T. Tsai, Y.B. Chen, Dielectric properties of $(1-y)$ $Ca_{1-x}La_{2x/3}TiO_3-y(Li,Nd)_{1/2}TiO_3$ ceramic system at microwave frequency, Materials Research Bulletin 36 (2001) 547–556.
[26] H.H.B. Rocha, F.N.A. Freire, M.R.P. Santos, J.M. Sasaki, T. Cordaro, A. S.B. Sombra, Radio-frequency (RF) studies of the magneto-dielectric composites: $Cr_{0.75}Fe_{1.25}O_3$(CRFO)–$Fe_{0.5}Cu_{0.75}Ti_{0.75}O_3$(FCTO), Physica B 403 (2008) 2902–2909.
[27] www.cryst.ehu.es.
[28] E.A.V. Ferri, J.C. Sczancoski, L.S. Cavalcante, E.C. Paris, J.W.M. Espinosa, A.T. de Figueiredo, P.S. Pizani, V.R. Mastelaro, J.A. Varela, E. Longo, Materials Chemistry and Physics 117 (2009) 192–198.
[29] C.H. Wang, X.P. Jing, W. Feng, J. Lu, Assignment of Raman-active vibrational modes of $MgTiO_3$, Journal of Applied Physics 104 (034112) (2008) 1–6.
[30] E. Cockayne, B.P. Burton, Phonons and static dielectric constant in $CaTiO_3$ from first principles, Phys. Rev. B 62 (2000) 3735–3743.
[31] T. Hirata, K. Ishioka, M. Kitajima, Vibrational spectroscopy and x-ray diffraction of perovskite compounds $Sr_{1-x}M_xTiO_3$ (M=Ca, Mg; $0 \le x \le 1$), Journal of Solid State Chemistry 124 (1996) 353–359.
[32] D. Borrow, T. Petroff, R. Tandon, M. Sayer, Characterization of thick lead zirconate titanate films fabricated using a new sol gel based process, Journal of Applied Physics 81 (876) (1997) 1–6.
[33] P. Sarah, S. Suryanarayana, Dielectric properties of piezoelectric 3–0 composites of lithium ferrite/barium titanate, Bulletin of Materials Science 26 (7) (2003) 745.
[34] I. Rychetsky, J. Petzelt, Dielectric spectra of grainy high-permittivity materials, Ferroelectrics 303 (2004) 137–140.
[35] Z. Hashin, S. Shtrikman, A variational approach to the theory of the effective magnetic permeability of multiphase materials, Journal of Applied Physics 33 (1962) 3125–3131.
[36] S. Kucheiko, J.W. Choi, H.J. Kim, H.J. Jung, Microwave dielectric properties of $CaTiO_3-Ca(Al_{1/2}Ta_{1/2})O_3$ ceramics, Journal of the American Ceramic Society 79 (1996) 2739–2743.
[37] A.E. Paladino, Temperature–compensated $MgTi_2O_5$–TiO_2 dielectrics, Journal of the American Ceramic Society 54 (1971) 168–169.
[38] C.L. Huang, C.H. Shen, Phase evolution and dielectric properties of $(Mg_{0.95}M^{2+}_{0.05})Ti_2O_5$ (M^{2+}=Co, Ni, and Zn) ceramics at microwave frequencies, Journal of the American Ceramic Society 92 (2009) 384–388.